nature physics

Article

https://doi.org/10.1038/s41567-022-01890-8

Time-of-flight quantum tomography of an atom in an optical tweezer

Received: 12 July 2022

Accepted: 23 November 2022

Published online: 23 January 2023

Check for updates

M. O. Brown [1,2] ✉, S. R. Muleady [1,2,3], W. J. Dworschack [1,2], R. J. Lewis-Swan [4,5], A. M. Rey [1,2,3], O. Romero-Isart [6,7] & C. A. Regal [1,2] ✉

A single particle trapped in a harmonic potential can exhibit rich motional quantum states within its high-dimensional state space. Quantum characterization of motion is key, for example, in controlling or harnessing motion in trapped ion and atom systems or observing the quantum nature of the vibrational excitations of solid-state objects. Here we show that the direct measurement of position and momentum can be used for quantum tomography of motional states of a single trapped particle. We obtain the momentum of an atom in an optical tweezer via time-of-flight measurements, which, combined with trap harmonic evolution, grants us access to all quadrature distributions. Starting with non-classical motional states of a trapped neutral atom, we demonstrate the Wigner function negativity and coherence of non-stationary states. Our work will enable the characterization of the complex neutral atom motion that is of interest for quantum information and metrology, and for investigations of the quantum behaviour of massive levitated particles.

The creation and full reconstruction of quantum states with genuine non-classical behaviour has played a key role in the development of quantum systems. Such reconstructions are perhaps most familiar in quantum optics as demonstrations of the quantum nature of light. In these experiments, state characterization has been accomplished both with homodyne tomography[1–4] and by coupling photons to a spin degree of freedom in cavity or circuit quantum electrodynamics (QED)[5,6]. The associated quasiprobability distributions that are obtained, such as the Wigner function, are useful tools for analysing non-classical behaviour. Although quasi-classical coherent states have strictly positive Wigner functions, other states, such as excited Fock states and Schrödinger cat states, can exhibit regions of negative phase-space density that have no classical analogue.

For particles with mass, the observation of non-classical states of motion is equally intriguing. Non-classical behaviour of a trapped particle was observed in seminal state generation and tomography of single ions harnessing a spin degree of freedom[7], and is of current interest, for example, in encoding trapped-ion qubits for error correction[8]. Increasingly, it is of interest to obtain quantum motional control over large mass objects both in the solid state[9–11] and for trapped dielectric particles[12,13]. Such large dielectric particles, and their control in the quantum regime in optical tweezers, are of interest in the search for electrical non-neutrality of matter, fundamental force law deviations, dark matter and in exploring the interplay between gravity and quantum mechanics[14,15]. It is now possible to cool the centre-of-mass motion of a dielectric particle to its quantum ground state[16–18], but lack of a controllable spin degree of freedom provides a barrier to quantum control and characterization. It has been proposed that a first proof of quantum behaviour of these objects is most naturally achieved using nonlinear potential landscapes and time-of-flight tomography[19,20]. Time-of-flight tomography requires not only measuring the momentum of the system of interest, but also harnessing coherent time evolution in the trap to rotate through the phase space spanned by both position and momentum[9]. This natural analogy to optical homodyne

[1]JILA, National Institute of Standards and Technology and University of Colorado, Boulder, CO, USA. [2]Department of Physics, University of Colorado, Boulder, CO, USA. [3]Center for Theory of Quantum Matter, University of Colorado, Boulder, CO, USA. [4]Homer L Dodge Dept of Physics and Astronomy, University of Oklahoma, Norman, OK, USA. [5]Center for Quantum Research and Technology, University of Oklahoma, Norman, OK, USA. [6]Institute for Theoretical Physics, University of Innsbruck, Innsbruck, Austria. [7]Institute for Quantum Optics and Quantum Information of the Austrian Academy of Sciences, Innsbruck, Austria. ✉e-mail: mark.o.brown@colorado.edu; regal@colorado.edu

https://doi.org/10.1038/s41567-022-01890-8

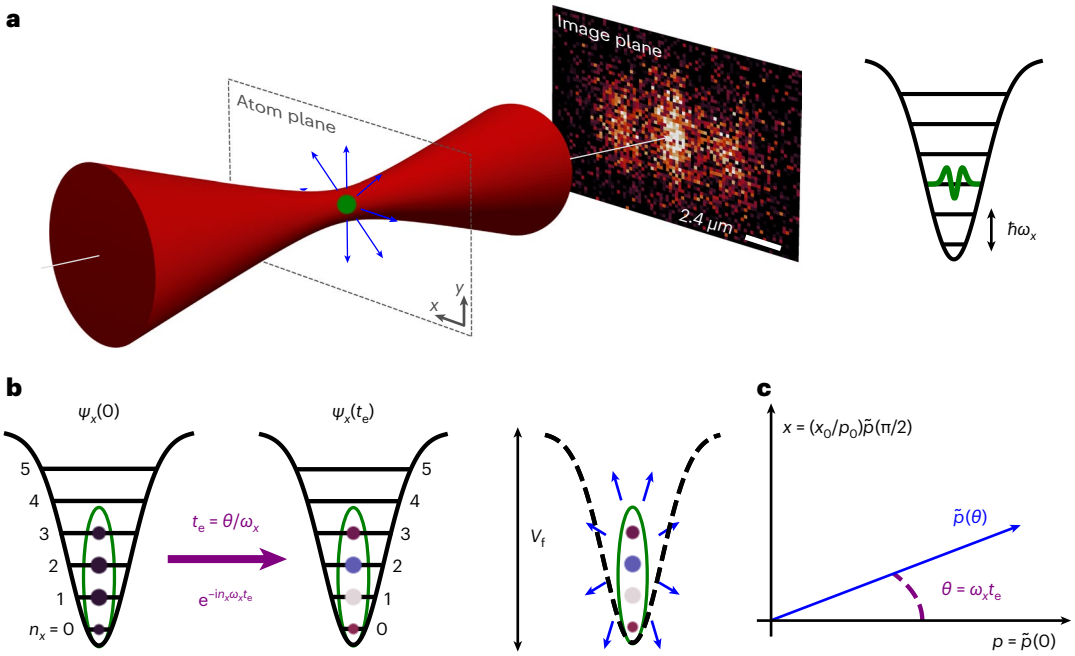

Fig. 1 | Tomography sequence and notation. a, Many time-of-flight images of a single atom released from the optical tweezer are averaged to measure the momentum distribution of a quantum state of motion. An example image of an $n_x = 2$ state is shown. **b**, A complex initial state (green ellipse) is prepared in an optical tweezer. Circle sizes and colours indicate example relative state populations and phases. The state evolves over a time t_e. The tweezer is turned off from a depth of V_f, and the atom expands in free space (blue arrows) for a fixed flight time t_f. **c**, The distribution measured after a given evolution time t_e in the trap, $\tilde{p}(\theta) = \tilde{p}(\omega_x t_e)$, is a generalized quadrature measurement of the initial state. At specific t_e, this generalized quadrature can be equivalent to the momentum quadrature $p = \tilde{p}(0)$ or the position quadrature $x = (x_0/p_0)\tilde{p}(\pi/2)$.

tomography has not been harnessed to characterize a non-classical state of a single trapped particle.

Time of flight is a long-standing technique in relation to atomic gases, lattices and beams[21–24]. So far, probing of motional quantum states using this technique has focused on single-quadrature ensemble properties of trapped atoms[25], tomography in atomic beam experiments[26], or the dynamics of collective modes of a gas[27]. For the microscopic control of single neutral atoms, optical tweezers have evolved into a versatile platform. In this context, time of flight may also be employed, and has been used, to measure thermal single atoms[28], and recently to probe spin correlations in few-fermion systems[29]. In this Article we harness single-atom sensitivity combined with measurements at multiple quadrature angles to carry out full tomography and reveal negative-valued Wigner functions in the harmonic oscillator state space of a single particle[19].

As illustrated in Fig. 1, to obtain a time-of-flight image we suddenly turn off the optical tweezer and allow the atom to fly in free space for a fixed time t_f. We then average many such images to determine the momentum distribution at the time of release. We extract arbitrary quadrature distributions by combining time-of-flight imaging with in-trap harmonic evolution for a time t_e (Fig. 1b,c). We start with a state $\psi_x(t_e = 0)$ that we want to characterize, and measuring this initial state via time of flight gives the momentum quadrature $\tilde{p}(t_e = 0) = p$. If we allow the atom with mass m to evolve in an ideal harmonic trap, the in-trap momentum after a time t_e is the rotated quadrature $\tilde{p}(\theta) = p\cos\theta + (p_0/x_0)x\sin\theta$ (Fig. 1c), where $\theta = \omega_x t_e$, and $x_0 = \sqrt{\hbar/(2m\omega_x)}$ and $p_0 = \sqrt{m\hbar\omega_x/2}$ are the characteristic length and momentum of the harmonic oscillator with angular frequency ω_x. By varying the evolution time t_e, we can extract an ensemble of quadrature distributions $\tilde{p}(\theta)$ for $\theta \in [0, 2\pi]$, analogous to what is done in optical homodyne tomography. The quadratures can be used to reconstruct the complete quantum state of the particle or the Wigner function $W(x, p)$. We note that, in terms of x_0 and p_0, the Heisenberg uncertainty relation takes the form $(\Delta x/x_0)(\Delta p/p_0) \geq 1$, where Δx and Δp are the root-mean-square (RMS) size of the corresponding Wigner function in phase space. For example, in these characteristic units, $\Delta x/x_0 = \sqrt{2n_x + 1}$ for Fock state $|n_x\rangle$.

In our experiments we test our protocol with multiple motional states, such as Fock states and displaced Fock states. To create the near-ground state of a single neutral ^{87}Rb atom, we use Raman sideband cooling[30]. To then create non-classical motional states, we use versatile control of quantum tunnelling in the optical tweezer[31]. This capability does not rely on internal states and spin–motion coupling as in standard trapped-ion settings[7,32], and hence can be extended to polarizable particles with no controlled internal degrees of freedom. With large mass dielectric particles, although quantum tunnelling is not experimentally feasible, it has been proposed that other non-harmonic potentials created by optical tweezers can enable quantum-state synthesis[20,27,33].

Our experiments start by stochastically loading single ^{87}Rb atoms into optical-tweezer traps using grey optical molasses and ascertaining the presence or absence of an atom through an initial in-trap fluorescence image. We then use optical molasses cooling followed by three-dimensional (3D) Raman sideband cooling in a trap of depth 1.0 mK to prepare the atom close to the three-dimensional motional ground state $|n_x, n_y, n_z\rangle = |0, 0, 0\rangle$ (Supplementary Information)[30]. The trap is then adiabatically ramped down to a depth of 0.33 μK where the remaining thermal population is allowed to escape to further purify the initial state.

In the first set of experiments, we measure the momentum distribution of motional states at $t_e = 0$ (Fig. 2). After preparing the state of interest, we adiabatically ramp the trap to a final depth $V_f/k_B = 2.4$ μK, where k_B is the Boltzmann constant, and then abruptly turn off the trap (Supplementary Information). We then wait for a flight time t_f before applying resonant light for $\tau = 10$ μs and collecting fluorescence on an electron-multiplying charge coupled device (EMCCD) camera through the 0.55-numerical aperture (NA) lens that creates the

https://doi.org/10.1038/s41567-022-01890-8

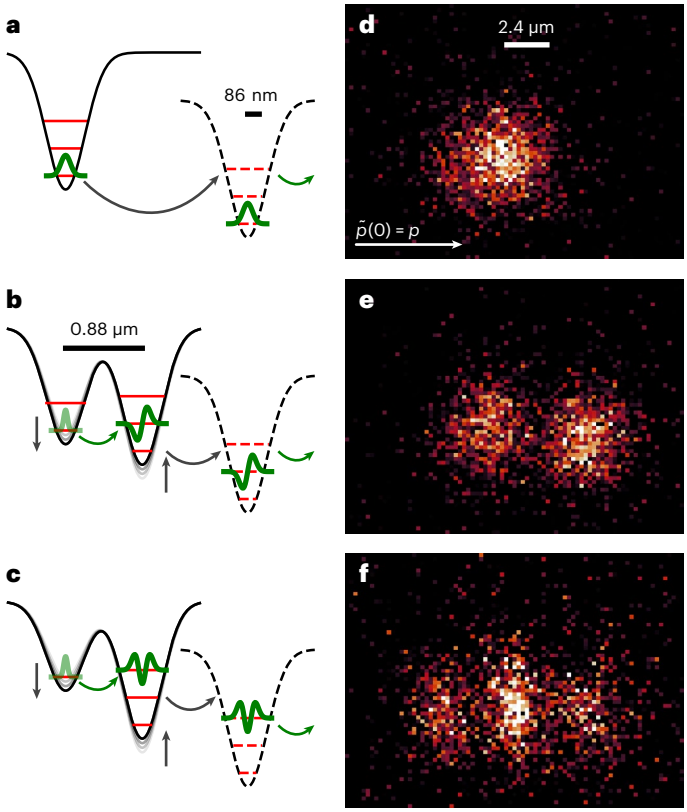

Fig. 2 | Single-atom Fock-state preparation and imaging. a–**c**, Illustration of motional state preparation of $n \in \{0, 1, 2\}$ states, respectively. **d**–**f**, Time-of-flight momentum distributions at $t_e = 0$ and for $t_f = 0.5$ ms of $n_x = (0, 1, 2)$ states for which (64,008, 48,309, 58,899) images were averaged, respectively.

optical tweezers. We repeat this procedure to realize multiple instances of single atom momentum measurements, and collect enough data to create an averaged momentum distribution that is observable above the camera noise. Experimental runs where an atom is not detected in the initial in-trap fluorescence image are used to characterize our imaging background, which is then subtracted from our captured momentum distribution (Supplementary Information).

We first characterize the expansion dynamics of an atom prepared close to the ground state of the optical tweezer with angular trap frequencies $\omega_{x,y,z}$ (Fig. 2a,b). The initial RMS size of the ground state in position space is estimated as $x_0 = 86$ nm, which is well below the resolution of our imaging system. At an expansion time of $t_f = 0.5$ ms, the atomic probability distribution has expanded to a RMS size of 2.4(1) μm, which is resolved by our imaging system (Fig. 2d). By studying the expansion as a function of flight time t_f, we can ascertain that the expansion's kinetic energy observed in the radial directions of $(k_B \times 0.256(16)\ \mu K)/2$ is partly driven by the expected zero-point kinetic energy of the harmonic oscillator, $E_{zp}/2 = \hbar\omega_{x,y}/4 = (k_B \times 0.188(1)\ \mu K)/2$ (Supplementary Information). The difference in energy is due to the finite temperature of the atoms, which can also be seen in Raman spectroscopy (Supplementary Information).

Starting with a ground-state atom, we create $n_x = 1$ or $n_x = 2$ motional Fock states using 1D tunnelling in a double well. The orientation of the double well during tunnelling breaks the radial symmetry of the tweezers, allowing us to only populate x-axis excited states (Supplementary Information). The tweezer is moved to 0.88 μm from a second empty optical tweezer on the right, and with both tweezers near a depth of 1.8 μK we bring the ground state of the left tweezer nearly energetically resonant with higher-n_x states of the right tweezer. Then, with an adiabatic sweep of the relative tweezer depths, the atom is transferred into the target excited state of the right tweezer (Fig. 2b,c; Supplementary Information)[31]. The two tweezers are then slowly separated and the intensity of the left tweezer is ramped to zero, releasing any atom that did not successfully transfer to avoid polluting the final image (Supplementary Information). We abruptly turn the remaining right tweezer off from 2.4 μK and proceed with the same imaging procedure as for the $n_x = 0$ state. The resulting $n_x = 1$ and $n_x = 2$ momentum distributions in Fig. 2e,f show the characteristic fringing that is expected of the excited motional states.

We now proceed to the full tomographic characterization of motional states. In these experiments, we study multiple quadrature distributions by waiting a variable amount of evolution time t_e before releasing the atom and imaging the result. We can visualize the quadrature data as time-sequence waterfall plots (Fig. 3a,d,g), which are derived from our raw distributions by deconvolving with the imaging point spread function (PSF) and integrating out the vertical axis (Supplementary Information). We study states with a goal of testing the capacity of time-of-flight tomography to identify non-classicality and phase preservation, as well as subtle non-stationary features. First, we create a coherent state by starting with an $n_x = 0$ state in the $V_f/k_B = 2.4$ μK trap and abruptly displacing the optical tweezer by 180 nm. We find that the state oscillates back and forth in the trap, as expected (Fig. 3a). Next, we produce an $n_x = 1$ Fock state using the same protocol as the data presented in Fig. 2b in a $V_f/k_B = 1.8$ μK trap. In addition, after the tunnelling and optical tweezer separation, the depth is suddenly doubled, resulting in application of a squeezing operation. This additional step, while reducing the fidelity of the $n_x = 1$ state slightly, is useful to characterize our ability to see nuanced behaviour in the tomography (Supplementary Information). The atom is then released from a trap of $V_f/k_B = 3.6$ μK. We observe that the state is mostly stationary, as expected, with the addition of a slight breathing from the squeezing induced by the depth jump (Fig. 3d). Finally, we combine multiple techniques by starting with an $n_x = 1$ state, applying the sudden doubling of the trap depth, and in addition displacing the optical tweezer by 140 nm. As shown in Fig. 3g, we are able to observe the expected oscillation dynamics of the state in the trap.

To reconstruct the quantum state from the quadrature data, we chose to use maximum likelihood estimation (MLE)[34] (Supplementary Information). An appropriately designed MLE algorithm takes the quadrature data and returns the density matrix that is most likely to reproduce the data[35]. We implemented an iterative MLE protocol based on the standard optical homodyne tomography literature[36], and from the density matrix, the Wigner function is recovered (Fig. 3).

The results of applying the MLE algorithm to the quadrature data are presented in Fig. 3b,c,e,f,h,i. The coherent state displays off-diagonal coherences but, as expected, a positive Wigner function (Fig. 3b,c). The non-Gaussian state preparation associated with Fig. 3d,g results in the density matrices and Wigner functions with negative values displayed in Fig. 3e,f. The value and statistical error on the density matrix and Wigner function negativity are estimated by a bootstrapping technique[36], in which we randomly sample predicted quadrature and noise distributions based on the MLE result and our camera noise characterization, respectively. We then extract the density matrices of these datasets to create a statistical ensemble of density matrices and Wigner functions (Supplementary Information). The nearly stationary $n_x = 1$ state displays a dominant $n_x = 1$ component and the Wigner minimum is found to be −0.060(6) where the value in parenthesis is the 1σ error based our bootstrapping technique (Fig. 3e). Adding a displacement demonstrates non-trivial off-diagonal coherences and a negative Wigner function value at the displaced centre of −0.064(6) (Fig. 3h,j).

A full assessment of the reconstructed wavefunction must also consider systematic errors, which we have studied in detail (Supplementary Information). Trap anharmonicity, for example, will result in measured quadratures that do not simply follow from the rotated quadratures of the ideal protocol. We determine the impact of

https://doi.org/10.1038/s41567-022-01890-8

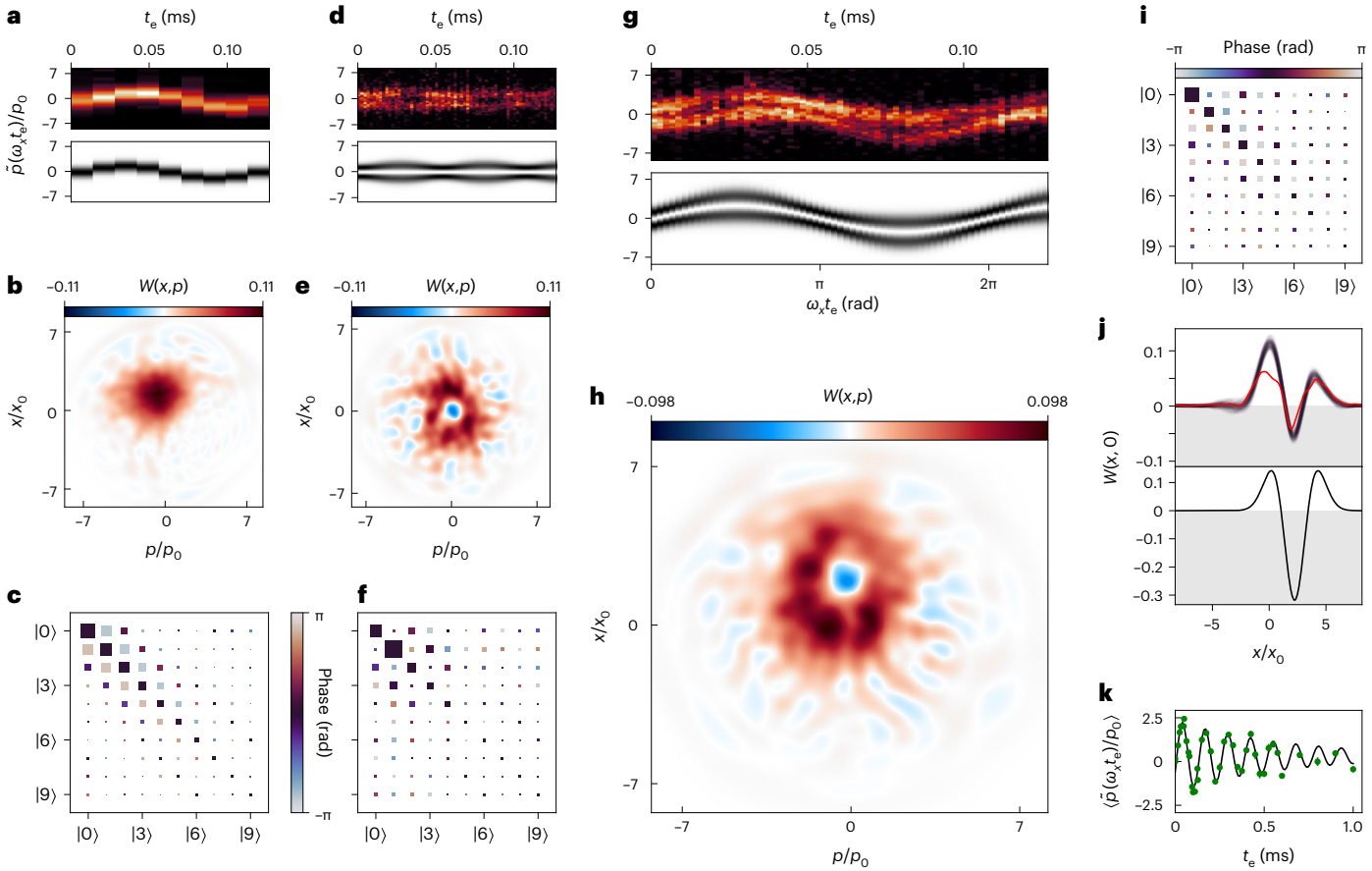

Fig. 3 | Motional quantum state tomography via time-of-flight imaging and maximum likelihood estimation. a–**i**, Measured quadrature data, Wigner functions and density matrix Hinton plots for the displaced $n_x = n_y = 0$ state (**a**–**c**), $n_x = 1$ state (**d**–**f**) and displaced $n_x = 1$ state (**g**–**i**). For the n_x=1 states, a slight squeezing operator is also applied. The quadrature data are presented as waterfall plots in **a**, **d** and **g**. Each vertical slice corresponds to a raw quadrature distribution, such as in Fig. 2, after deconvolving with the imaging PSF and integration along the vertical axis. The measured data (upper waterfall plot) are compared to the expectation for ideal preparation and harmonic time evolution based on our protocol (lower waterfall plot). The Wigner functions in **b**, **e** and **h** show classical positive values as red and non-classical negative values as blue. We normalize the Wigner function such that the ideal negativity of a pure $n_x = 1$ state is $-1/\pi$. The Hinton plots (**c**,**f**,**i**) for density matrices are reconstructed via MLE. The area of each square is proportional to the magnitude of the corresponding element's complex value, and the colour of the square represents the element's phase. For reference, the first four diagonal values in **f** are 0.21, 0.43, 0.12 and 0.065. **j**, The $p = 0$ slice of reconstructed Wigner functions from **h** (red), and equivalent slices as reconstructed through a bootstrapping method (dark purple) that characterize the statistical uncertainty of our reconstruction algorithm (upper diagram). The perfect displaced and squeezed $n = 1$ state (black) is shown for comparison to experimental data (lower diagram). **k**, Evolution of the measured centre of the coherent state (green circles) and damped sinusoidal fit (black line), which is used to characterize the trap frequency and anharmonicity.

anharmonicity by theoretically assessing the tomography protocol based on a model using measured trap parameters. We estimate our trap anharmonicity by studying the coherent state oscillations of Fig. 3a over a longer time (Fig. 3k). The centre of the Gaussian oscillates at 7.84(5) kHz, and decays with a time constant of 0.63(14) ms. A model of the trap containing an anharmonic term is fitted to match the observed damping. For a displaced $n_x = 1$ state in this model, we compare the reconstructed states obtained from MLE after evolution in a trap with and without our modelled anharmonic terms. We observe only a small infidelity of <5% between the resulting reconstructed states, and the Wigner function minimum for anharmonic evolution is smaller in magnitude by <0.01 compared to harmonic evolution, and remains negative (Supplementary Information). In the future, the large dynamic range and control afforded by optical traps can be used to control the harmonicity. Specifically, a shallow double-well or other anharmonic traps could be used for state creation, and the tomography could be carried out after ramping to a much deeper and less anharmonic trap.

We have demonstrated quantum tomography of non-classical single-atom motional states. By using time-of-flight imaging, we have measured negative-valued Wigner functions with non-trivial phase-space structure for a single atom. This work lays the foundation for tomography and characterization of massive levitated particles without exploitable spin structure[15,20,37]. Furthermore, our work expands the horizon of the study of motion in neutral atom systems. Time-of-flight tomography can be directly extended to the study of high-n motional superposition states[38], highly squeezed states and interference of complex delocalized states[39]. Motional control and preservation is a component of the pursuit of high-fidelity Rydberg gates[40], and phonons may even become useful as a long-lived harmonic oscillator resource in neutral atom systems. For both cases, full state characterization is an elucidating capability. In the context of multi-particle dynamics, the ability to fully characterize the single-particle wavefunction via time-of-flight tomography of individual particles, as well as to access detailed information regarding higher-order momentum and spatial correlators, will open up complementary capabilities to more thoroughly survey the complex nature of quantum many-body states[41,42]. Such possibilities include determining the degree of non-separability arising from the interplay of interactions and quantum statistics, as well as certifying and quantifying different types of entanglement present in few-body systems.

Online content

Any methods, additional references, Nature Portfolio reporting summaries, source data, extended data, supplementary information, acknowledgements, peer review information; details of author contributions and competing interests; and statements of data and code availability are available at https://doi.org/10.1038/s41567-022-01890-8.

References

1. Vogel, K. & Risken, H. Determination of quasiprobability distributions in terms of probability distributions for the rotated quadrature phase. *Phys. Rev. A* **40**, 2847–2849 (1989).
2. Smithey, D. T., Beck, M., Raymer, M. G. & Faridani, A. Measurement of the Wigner distribution and the density matrix of a light mode using optical homodyne tomography: application to squeezed states and the vacuum. *Phys. Rev. Lett.* **70**, 1244–1247 (1993).
3. Lvovsky, A. I. et al. Quantum state reconstruction of the single-photon Fock state. *Phys. Rev. Lett.* **87**, 050402 (2001).
4. Gross, C. et al. Atomic homodyne detection of continuous-variable entangled twin-atom states. *Nature* **480**, 219–223 (2011).
5. Deleglise, S. et al. Reconstruction of non-classical cavity field states with snapshots of their decoherence. *Nature* **455**, 510–514 (2008).
6. Hofheinz, M. et al. Synthesizing arbitrary quantum states in a superconducting resonator. *Nature* **459**, 546–549 (2009).
7. Leibfried, D. et al. Experimental determination of the motional quantum state of a trapped atom. *Phys. Rev. Lett.* **77**, 4281–4285 (1996).
8. Flühmann, C. et al. Encoding a qubit in a trapped-ion mechanical oscillator. *Nature* **566**, 513–517 (2019).
9. Dunn, T., Walmsley, I. & Mukamel, S. Experimental determination of the quantum-mechanical state of a molecular vibrational mode using fluorescence tomography. *Phys. Rev. Lett.* **74**, 884–887 (1995).
10. O'Connell, A. D. et al. Quantum ground state and single-phonon control of a mechanical resonator. *Nature* **464**, 697–703 (2010).
11. Chu, Y. et al. Creation and control of multi-phonon Fock states in a bulk acoustic-wave resonator. *Nature* **563**, 666–670 (2018).
12. Chang, D. E. et al. Cavity opto-mechanics using an optically levitated nanosphere. *Proc. Natl Acad. Sci. USA* **107**, 1005–1010 (2010).
13. Romero-Isart, O., Juan, M. L., Quidant, R. & Cirac, J. I. Toward quantum superposition of living organisms. *N. J. Phys.* **12**, 033015 (2010).
14. Moore, D. C. & Geraci, A. A. Searching for new physics using optically levitated sensors. *Quantum Sci. Technol.* **6**, 014008 (2021).
15. Gonzalez-Ballestero, C., Aspelmeyer, M., Novotny, L., Quidant, R. & Romero-Isart, O. Levitodynamics: levitation and control of microscopic objects in vacuum. *Science* **374**, eabg3027 (2021).
16. Delić, U. et al. Cooling of a levitated nanoparticle to the motional quantum ground state. *Science* **367**, 892–895 (2020).
17. Tebbenjohanns, F., Mattana, M. L., Rossi, M., Frimmer, M. & Novotny, L. Quantum control of a nanoparticle optically levitated in cryogenic free space. *Nature* **595**, 378–382 (2021).
18. Magrini, L. et al. Real-time optimal quantum control of mechanical motion at room temperature. *Nature* **595**, 373–377 (2021).
19. Romero-Isart, O. et al. Optically levitating dielectrics in the quantum regime: theory and protocols. *Phys. Rev. A* **83**, 013803 (2011).
20. Weiss, T. & Romero-Isart, O. Quantum motional state tomography with nonquadratic potentials and neural networks. *Phys. Rev. Res.* **1**, 033157 (2019).
21. Greiner, M., Mandel, O., Esslinger, T., Hänsch, T. W. & Bloch, I. Quantum phase transition from a superfluid to a Mott insulator in a gas of ultracold atoms. *Nature* **415**, 39–44 (2002).
22. Schellekens, M. et al. Hanbury Brown Twiss effect for ultracold quantum gases. *Science* **310**, 648–651 (2005).
23. Bloch, I., Dalibard, J. & Zwerger, W. Many-body physics with ultracold gases. *Rev. Mod. Phys.* **80**, 885–964 (2008).
24. Bücker, R. et al. Twin-atom beams. *Nat. Phys.* **7**, 608–611 (2011).
25. Morinaga, M., Bouchoule, I., Karam, J.-C. & Salomon, C. Manipulation of motional quantum states of neutral atoms. *Phys. Rev. Lett.* **83**, 4037–4040 (1999).
26. Kurtsiefer, C., Pfau, T. & Mlynek, J. Measurement of the Wigner function of an ensemble of helium atoms. *Nature* **386**, 150–153 (1997).
27. Bücker, R. et al. Vibrational state inversion of a Bose-Einstein condensate: optimal control and state tomography. *J. Phys. B At. Mol. Opt. Phys.* **46**, 104012 (2013).
28. Fuhrmanek, A. et al. Imaging a single atom in a time-of-flight experiment. *N. J. Phys.* **12**, 053028 (2010).
29. Bergschneider, A. et al. Experimental characterization of two-particle entanglement through position and momentum correlations. *Nat. Phys.* **15**, 640–644 (2019).
30. Kaufman, A. M., Lester, B. J. & Regal, C. A. Cooling a single atom in an optical tweezer to its quantum ground state. *Phys. Rev. X* **2**, 041014 (2012).
31. Kaufman, A. M. et al. Entangling two transportable neutral atoms via local spin exchange. *Nature* **527**, 208–211 (2015).
32. Kienzler, D. et al. Quantum harmonic oscillator state synthesis by reservoir engineering. *Science* **347**, 53–56 (2015).
33. Ciampini, M. A. et al. Experimental nonequilibrium memory erasure beyond Landauer's bound. Preprint at https://arxiv.org/abs/2107.04429 (2021).
34. Leonhardt, U. *Measuring the Quantum State of Light* 1st edn (Cambridge Univ. Press, 1997).
35. Banaszek, K., D'Ariano, G. M., Paris, M. G. A. & Sacchi, M. F. Maximum-likelihood estimation of the density matrix. *Phys. Rev. A* **61**, 010304 (1999).
36. Lvovsky, A. I. Iterative maximum-likelihood reconstruction in quantum homodyne tomography. *J. Opt. B Quantum Semiclassical Opt.* **6**, S556 (2004).
37. Vanner, M., Hofer, J., Cole, G. & Aspelmeyer, M. Cooling-by-measurement and mechanical state tomography via pulsed optomechanics. *Nat. Commun.* **4**, 2295 (2013).
38. McCormick, K. C. et al. Quantum-enhanced sensing of a single-ion mechanical oscillator. *Nature* **572**, 86–90 (2019).
39. Parazzoli, L. P., Hankin, A. M. & Biedermann, G. W. Observation of free-space single-atom matter wave interference. *Phys. Rev. Lett.* **109**, 230401 (2012).
40. Weiss, D. S. & Saffman, M. Quantum computing with neutral atoms. *Phys. Today* **70**, 44 (2017).
41. Asteria, L., Zahn, H. P., Kosch, M. N., Sengstock, K. & Weitenberg, C. Quantum gas magnifier for sub-lattice-resolved imaging of 3D quantum systems. *Nature* **599**, 571–575 (2021).
42. Holten, M. et al. Observation of Cooper pairs in a mesoscopic two-dimensional Fermi gas. *Nature* **606**, 287–291 (2022).

Methods

Tweezer generation and control

The optical tweezers were generated by sending light at a wavelength of 850 nm through two orthogonal Intraaction ATD-1803DA2.850 acousto-optic deflectors (AODs), which were driven simultaneously with multiple radiofrequency (RF) tones to create multiple deflections. The horizontal AOD was used to generate the two deflections used for tunnelling, to avoid complications arising from gravity. The vertical AOD was used to direct extra laser power far away from the main tweezers holding atoms, enabling reduction of the depth of the main tweezers by many orders of magnitude, even with a limited-intensity servo dynamic range. The relative depths of the traps were modified by dynamically adjusting the amount of RF power in each tone driving the horizontal AOD. The tweezers were moved by changing the frequencies of the RF tones driving the AODs. The Supplementary Information provides a summary of all time sequences.

We used a stochastic ΛGM process to load a $V/k_B = 0.58$ mK deep trap. The loading technique we used is capable of up to ~90% loading efficiency[43]. However, because interleaving background images, in which no atom is initially loaded, provides useful information, we used sub-optimal loading at 50–80% efficiency.

Imaging

The camera used was an Andor IXON-EM+ back-illuminated EMCCD camera (model no. DU-897E-C00-#BV-9GT). The 780-nm imaging light was collected through the same high-NA objective lens used to create our tweezer array and split from the optical tweezer light using a dichroic mirror. We set the objective to NA = 0.55 and measured the optical-tweezer trap parameters that corroborated this value. Supplementary Information discusses the camera noise and artefacts in detail, as well as the motional tomography analysis.

The imaging light applied during time of flight was near-resonant and operated with intensity $I \gg I_{sat}$ during the pulse of duration $\tau = 10$ μs. The light was applied in a power-balanced σ_+, σ_- polarization configuration on the D_2 $F = 2$ to $F' = 3$ ^{87}Rb transition.

Red-detuned polarization gradient cooling (RPGC) and the associated light scattering was used to determine the presence or absence of the atom at the start of the experiment. Time-of-flight images were post-selected based the presence of an atom in the RPGC image. Some time-of-flight images that recorded cosmic ray events were additionally removed in post-selection. The RPGC cooling was in a balanced, $\sigma^+ - \sigma^-$ configuration with zero background magnetic field. During the imaging, we alternated trap light and imaging light at a 2-MHz flashing rate[44,45]. This eliminated light shifts and anti-trapping effects during the scattering of the imaging light to create more uniform images.

Data availability

The data that support plots and other findings in this paper are available from the authors on reasonable request.

References

43. Brown, M. O., Thiele, T., Kiehl, C., Hsu, T.-W. & Regal, C. A. Gray-molasses optical-tweezer loading: controlling collisions for scaling atom-array assembly. *Phys. Rev. X* **9**, 011057 (2019).
44. Hutzler, N. R., Liu, L. R., Yu, Y. & Ni, K.-K. Eliminating light shifts for single atom trapping. *N. J. Phys.* **19**, 023007 (2017).
45. Lester, B. J. et al. Measurement-based entanglement of noninteracting bosonic atoms. *Phys. Rev. Lett.* **120**, 193602 (2018).

Acknowledgements

We thank T. Thiele, S. Pampel and T.-W. Hsu for valuable insights and technical assistance, and K. Lehnert and A. Kaufman for input on the manuscript. We acknowledge funding from NSF grant PHYS 1734006, ONR grants N00014-17-1-2245 and N00014-21-1-2594, NSF QLCI award OMA 2016244, and the US Department of Energy, Office of Science, National Quantum Information Science Research Centers, Quantum Systems Accelerator, and the Baur-SPIE Endowed Professor at JILA. W.J.D. acknowledges support from an NSF Graduate Fellowship.

Author contributions

M.O.B., A.M.R., O.R.-I. and C.A.R. conceived and designed the experiments. M.O.B. and W.J.D. performed the experiments. M.O.B., S.R.M., W.J.D. and C.A.R. analysed the data. M.O.B., S.R.M., W.J.D., R.J.L.-S., A.M.R., O.R.-I. and C.A.R. contributed materials/analysis tools. M.O.B., S.R.M., W.J.D., R.J.L.-S., A.M.R., O.R.-I. and C.A.R. wrote the paper.

Competing interests

The authors declare no competing interests.

Additional information

Supplementary information The online version contains supplementary material available at https://doi.org/10.1038/s41567-022-01890-8.

Correspondence and requests for materials should be addressed to M. O. Brown or C. A. Regal.

Peer review information *Nature Physics* thanks Hannes Bernien and the other, anonymous, reviewer(s) for their contribution to the peer review of this work.